International Symposium
On Turbulence and Shear Flow
Phenomena (TSFP-9)
June 30 - July 3, 2015 Melbourne, Australia

Active drag reduction in a turbulent boundary layer based on plasma-actuator-generated streamwise vortices

Chi Wai Wong, Yu Zhou, Yinzhe Li and Yupeng Li

Institute for Turbulence-Noise-Vibration Interactions and Control
Shenzhen Graduate School, Harbin Institute of Technology
Shenzhen 518055, P.R. China
Email: cwwong@hitsz.edu.cn

ABSTRACT

This work aims to manipulate a fully developed turbulent boundary layer (TBL) over a flat plate for drag reduction based on plasma-induced streamwise vortices. Four different plasma actuator configurations are explored for generating streamwise vortices. A surface balance technique is deployed to measure the skin-friction drag, along with a new calibration method, to resolve accurately the friction drag change. It is found that the plasma-actuator-generated vortices and their interactions with the boundary layer may lead to a substantial drag reduction. The control efficiency is also estimated. The hotwire, flow visualization and PIV data all point to a pronounced change in the flow structure of the manipulated boundary layer.

INTRODUCTION

Active drag reduction of turbulent boundary layers has received a great attention in the literature due to its practical and fundamental importance.

Dielectric barrier discharge (DBD) plasma actuator is a relatively new active control device but is experiencing a rapid development due to its simple structure, rapid response and no moving parts. Furthermore, it is efficient for imparting momentum to the flow much like blowing or suction, though without mass injection. The simplest arrangement of DBD plasma actuator typically consists of a pair of electrodes separated by dielectric material, and an alternating voltage is applied across the electrodes, resulting in the generation of plasma in the vicinity of the electrodes. The voltage difference applied between the electrodes may vary between 1 and 10 $kV_{p\text{-}p}$ (subscript p-p denotes the peak-to-peak), and the frequency of the driving voltage is typically from 1 to 10 kHz (Font, 2006; Jukes, 2006). The electrical properties and induced thrust of plasma actuator are summarized by Enloe et al. (2004a, 2004b). Plasma actuator is rather extensively used for the laminar and turbulent flow separation control on streamlined and bluff bodies. See Moreau (2007) and Corke et al. (2010) for recent reviews on plasma actuators for aerodynamic applications. Choi et al. (2011) studied two configurations of plasma actuators for the control of a turbulent boundary layer over a flat plate. Their plasma actuators were aligned in the streamwise direction to produce forcing along the spanwise direction. Both spanwise oscillation and spanwise travelling waves could be produced, depending on the direction of the induced flow of each actuator. Their manipulation modified the near-wall structures. They suggested that the spanwise oscillation and travelling waves generated could lead to a drag reduction by 45%, though the drag change was not measured in their investigation.

In spite of extensive investigations, many aspects of skin friction drag reduction based on plasma actuators have yet to be clarified. For examples, how do the plasma-actuator-induced streamwise vortices interact with the near-wall structures? How does the applied voltage on plasma actuators influence the drag change? The first objective of this work is to investigate experimentally how the plasma configurations may influence the drag reduction in a turbulent boundary layer over a flat plate. To this end, four DBD plasma-actuator configurations are deployed for the generation of streamwise vortices and a new calibration method is proposed for the surface balance technique to resolve accurately the friction drag change. The second objective of this work is to examine the flow structure change that is associated with a substantial decrease in skin friction drag under the minipulation of plasma actuators, and hopefully to gain an improved understanding of drag reduction mechanisms. The hotwire, smoke-wire flow visualization and PIV techniques are used to measure the boundary layer with and without control.

EXPERIMENTAL DETAILS

Experiments were performed in a closed-loop wind tunnel, with a test section of $L \times W \times H = 5.5 \times 0.8 \times 1.0$ m. A rounded leading-edge flat plate with $L \times W \times H = 4.8 \times 0.78 \times 0.015$ m was installed vertically in the test section, and an adjustable end plate was used to ensure zero pressure gradient. Two rows of screws were installed at $x = 100$ mm downstream of the leading-edge of the flat plate to generate fully developed turbulent boundary-layer at the measurement station ($x = 3.2$ m) in the free-stream velocity U_∞ of 2.4 m/s. The boundary layer thickness δ was 85 mm at the measurement station, while the Reynolds number $Re_\theta = 1100$ based on the momentum thickness θ, and the wall unit length $l = 150$ μm without perturbation.

The DBD plasma actuators consist of two copper electrodes separated by a dielectric panel, which gave an overall thickness of about 230 μm ($\approx 1.5l$). Plasma was generated by applying a sinusoidal AC waveform to the

upper electrodes with voltage E = 3.00 - 7.84 $kV_{p\text{-}p}$ at frequencies f = 11 kHz, with the lower electrodes connected to ground. Four different plasma actuators, i.e., configurations A, B, C and D (Fig. 1), are investigated. A is characterized by colliding counter-rotating vortices, and the streamwise vortex induced by one plasma actuator collides with that by the adjacent one along the entire length of the actuator. B is a counter-rotating vortex generator where the two streamwise vortices do not collide with each other. C is a non-colliding co-rotating vortex generator. D is a sawtooth plasma actuator, which induces streamwise flow and one counter-rotating vortex pair at the tip and between the tips, respectively.

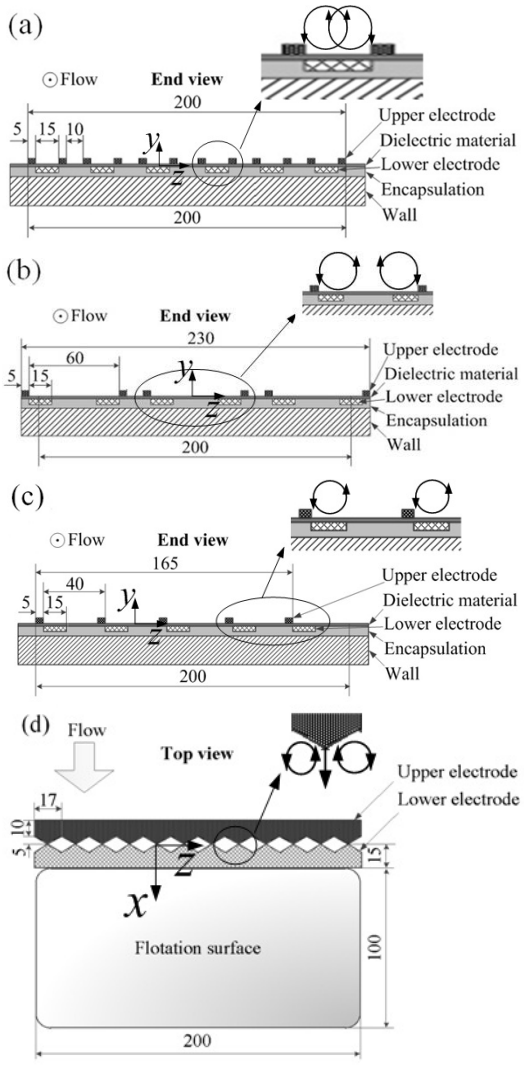

Figure 1. Four plasma configurations: (A); (B); (C); (D).

A custom-built surface balance is designed, based on Krogstad and Efros (2010), to measure the averaged skin-friction drag over an area covering 0.2 m × 0.1 m = 0.02 m^2 at x = 3.2 m (Fig. 2). The skin-friction drag on the flotation surface is resolved using the lever principle. The amplified force is measured by a load cell (Honeywell M34, range ±1kg). A calibration method is presently proposed for the surface balance. Firstly, measure the velocity profile at the measurement station at U_∞ = 2.4 and 5 m/s using a hotwire. Secondly, fit the velocity profile to the logarithmic portion of the universal velocity profile. The friction velocity u_τ is then determined from Eq. (1) and the skin-friction drag F is estimated from Eq. (2).

$$\frac{\overline{U}}{u_\tau} = 2.44\ln\left(\frac{u_\tau}{\overline{U}}\right) + 2.44\ln\left(\frac{\overline{U}y}{\nu}\right) + 4.9 \qquad (1)$$

$$F = \rho u_\tau^2 A \qquad (2)$$

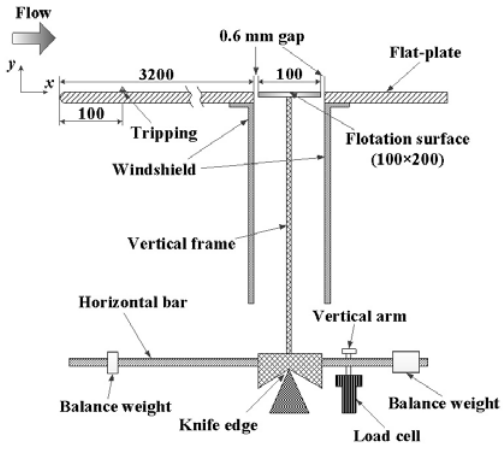

Figure 2. Schematic of experimental setup for skin friction measurement using surface balance.

A single hotwire of 5 μm in diameter and about 1 mm in length is traversed, normally to the wall, across the boundary layer to measure the streamwise mean velocity profile with a resolution of 10 μm. Smoke-wire flow visualization is conducted in the x-z plane at y^+ = 24 with and without control. Note that x, y and z are defined as the streamwise, wall-normal and spanwise directions, and the origin is defined at the mid point and the trailing edge of the actuators (e.g. Fig. 1b). The smoke wire is placed at y^+ = 20 and 150 mm downstream of the leading-edge of the plasma actuators, parallel to the wall and normal to the free stream. The laser sheet is at y^+ = 24, parallel to the wall. A Dantec time-resolved PIV system is used to measure the turbulent boundary layer in the x-z (y^+ = 24) and x-y (z^+ = 133) planes with and without control. The PIV measurement in the x-y plane was chosen at z^+ = 133, where the spanwise distribution of the local drag reduction is a maximum, as found out from the hotwire measurement. The incoming flow is seeded with smoke generated from peanut oil by a TSI 9307-6 particles generator. The averaged seeding particle diameter is about 1 μm. A dual beam laser system (Litron LDY304-PIV, Nd:

YLF), with a maximum energy output of 30 mJ/pulse, is used in conjunction with spherical and cylindrical lenses to form a thin light sheet of approximately 0.8 mm thick. Particle images are captured by a CCD camera (double frames, 2560 pixels × 1600 pixels). The sampling rate is 200 frames per second and the sampling duration is 5 s.

RESULTS AND DISCUSSION

Control performance

Figure 3 shows the dependence of drag change $\Delta c_f = (F_1-F_2)/F_2$ on voltage for different plasma configurations, where F_1 and F_2 are the skin-friction drags with and without plasma operated, respectively. Note that, due to a difference in the electrode geometry and hence total "effective" length between plasma configurations, the comparison in Fig. 3a is based on different power consumption.

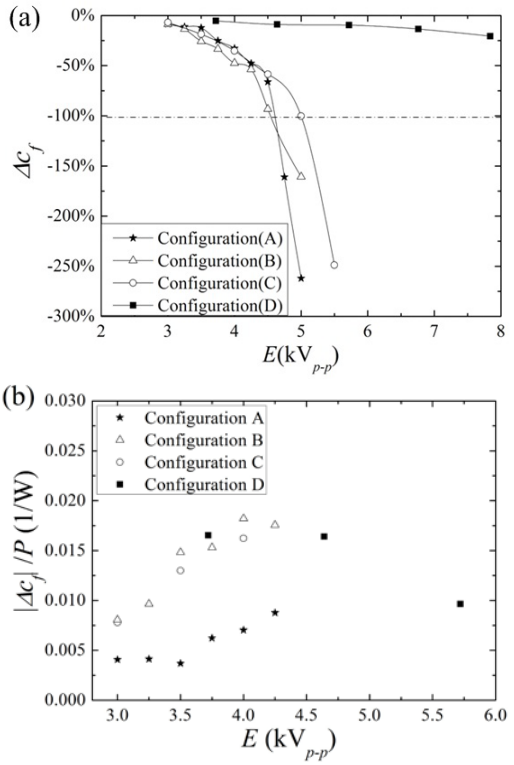

Figure 3. (a) Dependence of Δc_f on voltage E; (b) Dependence of the control efficiency $|\Delta c_f|/P$ on E.

For configurations A, B and C, Δc_f increases rapidly with increasing voltage, particularly at $E \leq 4.25$ $\mathrm{kV}_{p\text{-}p}$ (Fig. 3a). The Δc_f of B is always slightly larger than that of A or C. The induced vortex pair for A forms an upwash region upon collision, whilst streamwise vortices generated for B and C do not collide with each other due to large spanwise spacing between plasma actuators. The slope of the curves increases suddenly at $E = 4.25$ $\mathrm{kV}_{p\text{-}p}$ for A, B and C, indicating the occurrence of flow separation and reversal, which leads to Δc_f shooting over -100%. In contrast, the flow separation does not occur for D, whose Δc_f is significantly lower than others though.

The control efficiency, $|\Delta c_f|/P$ is examined in Fig. 3b, where P is the total electrical power consumption of the actuator. Note that Δc_f is negative for the drag reduction. Therefore, $|\Delta c_f|$ is used to calculate the control efficiency. Configuration A shows the lowest control efficiency of all, whereas B and C are virtually the same. In general, the $|\Delta c_f|/P$ increases initially for higher voltage. But beyond a certain level of voltage, $|\Delta c_f|/P$ drops, probably because higher voltage produces flow separation in cases of B and C or the streamwise flow induced at the tip of the sawtooth electrode induces significant additional drag in case of configuration D. The data at $E > 4.5$ $\mathrm{kV}_{p\text{-}p}$ has been removed for A, B and C in view of the occurrence of flow separation and reversal.

Modified flow structure

In view of the fact that configuration B gives the best control efficiency compared with others, the data obtained for this configuration is presented to illustrate the modified flow structure.

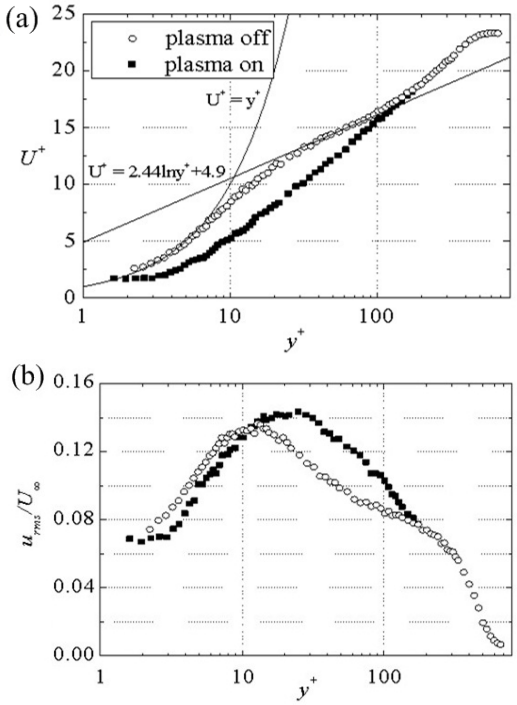

Figure 4. Distributions of (a) mean streamwise velocity U^+ and (b) turbulent intensity u_{rms}/U_∞ for the natural and controlled cases ($z^+ = 133$).

There is a decrease in the mean streamwise velocity U^+ up to $y^+ \approx 100$ (Fig. 4a). The turbulent intensity u_{rms}/U_∞ is reduced at $y^+ < 10$ but increased at $10 < y^+ < 160$ (Fig. 4b), compared with the uncontrolled TBL. The

typical images of instantaneous flow structure (y^+ = 24) show the high- and low-speed streaks without control (Fig. 5a). Note that the low speed streaks appear pushed toward the centre of the actuator pair in the presence of control (Fig. 5b). The low-speed streaks appear stabilized, which is consistent with the substantially reduced drag. Two high-speed fluid regions occur on each side of the region of low-speed streaks, as a result of the downwash flow due to the plasma-induced rotating vortices (not shown).

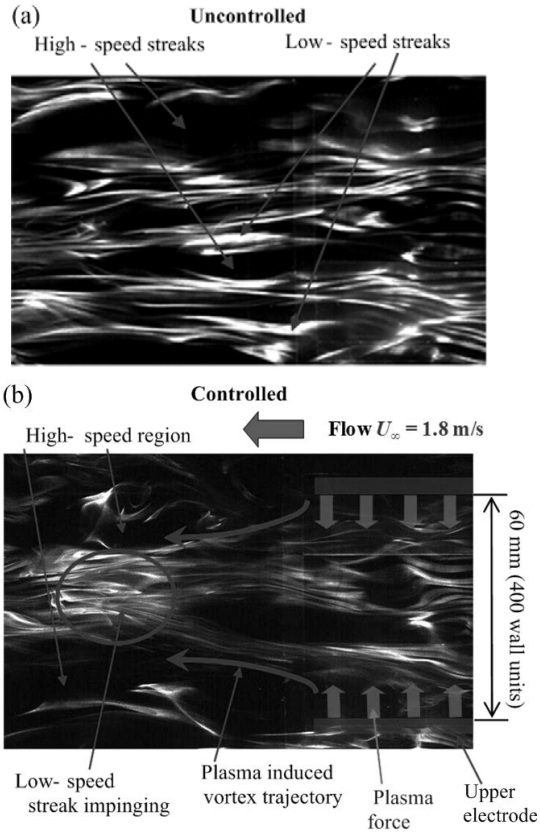

Figure 5. Smoke-wire flow visualization of instantaneous flow structure at y^+ = 24 for (a) natural and (b) manipulated flow with control. The smoke wire and laser sheet are positioned at y^+ = 20 and 24, respectively.

Figure 6 presents the energy dissipation spectrum at various y^+ (x^+ = 167, z^+ = 133) with and without control, obtained by multiplying the power spectral density function E_u of streamwise fluctuating velocity u by f^{+2} (e.g. Mydlarski and Warhaft, 1996). Note that the integral of the energy dissipation spectrum yields the energy dissipation rate $(\partial u^+/\partial x^+)^2$. Once the control is applied, $(\partial u^+/\partial x^+)^2$ is considerably larger than that without control at $y^+ \leq 10$ but is essentially unchanged at y^+ = 100. This may suggest that the plasma-actuator-generated vortices may have enhanced greatly the energy dissipation rate in the near wall region, which is consistent with the substantially reduced drag.

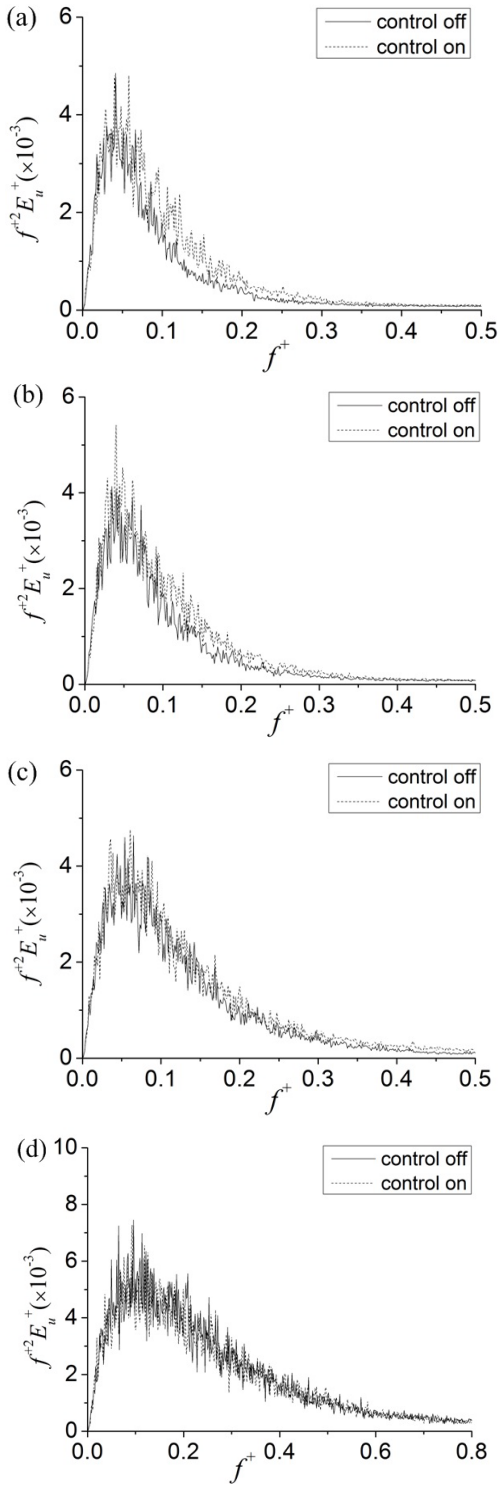

Figure 6. Energy dissipation spectra at (a) (x^+, y^+, z^+) = (167, 3.3, 133), (b) (167, 4.6, 133), (c) (167, 10, 133), and (d) (167, 102, 133) for configuration B.

Figure 7 shows the Taylor microscale, defined by $\lambda_T = \sqrt{\overline{2u^2}/\overline{(\partial u/\partial t)^2}}$, which contains information on both the large scales, $\overline{u^2}$, and small scales, $\overline{(\partial u/\partial t)^2}$. In the absence of control, $\lambda_T{}^+$ increases to the maximum (≈ 9.1) at $y^+ \approx 5$. At $y^+ > 5$, $\lambda_T{}^+$ decreases with increasing y^+, which is consistent with the results of Metzger et al. (2004). With control, the $\lambda_T{}^+$ is smaller than that of the uncontrolled case in the sublayer and part of the buffer region. At $y^+ \approx 5$, the maximum $\lambda_T{}^+$ is 8. Based on Tardu (2001), the decreased $\lambda_T{}^+$ under control indicates an increase in the energy dissipation rate and also an energy transfer from the large-scale to small-scale structures.

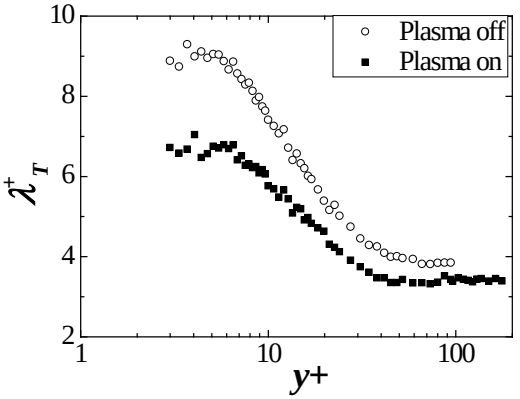

Figure 7. Variations with y^+ in the Taylor microscale $\lambda_T{}^+$ for configuration B at (x^+, y^+, z^+) = (167, y^+, 133).

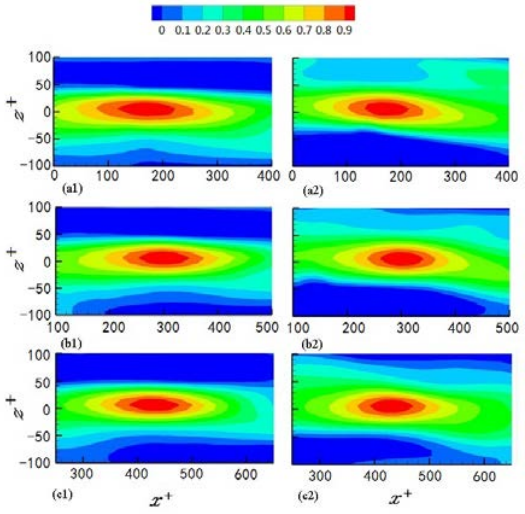

Figure 8. Two-point velocity correlation coefficient R_{uu} in the x-z plane (y^+ = 24) for plasma off (left column) and on (right column). The reference point is (x^+, z^+) = (167, 0) in (a1, a2), (300, 0) in (b1, b2) and (433, 0) in (c1, c2).

Two-point correlations of the velocity fluctuations are examined based on the PIV data, from which the length scales associated with the near-wall streaky structures and streamwise vortices can be estimated (Bhaganagar et al., 2004). The iso-contours of the two-point velocity correlation coefficient R_{uu} ($=\frac{1}{T}\int_0^T u(A)u(B)dt$, where $u(A)$ and $u(B)$ are the streamwise fluctuating velocity at points A and B, T is the sample time) in the x-z plane (y^+ = 24) show an elliptical shape due to the strong anisotropy between the streamwise and spanwise directions, with and without control. Under control, the R_{uu}-contours for each x^+ location shrinks longitudinally, indicating shortened streaky structures, but grows in spanwise direction for R_{uu} < 0.5. The observation is consistent with increased separation between low-speed streaks.

The probability density functions (PDF) of the wall-normal vorticity $\omega_y/\omega_y{}'$ calculated from the PIV data measured in the x-z plane (y^+ = 24), are compared for the natural and manipulated turbulent boundary layer behind the trailing edge of the actuators (Fig. 9), where $\omega_y{}'$ is the root mean square value of ω_y in the absence of control. The PDF increases significantly about $\omega_y/\omega_y{}'$ = 0 but decreases in the region of $\omega_y \geq \omega_y{}'$ and $\omega_y \leq -\omega_y{}'$. This suggests a suppressed strength of near wall streaky structures, which is consistent with the reduced wall shear stress.

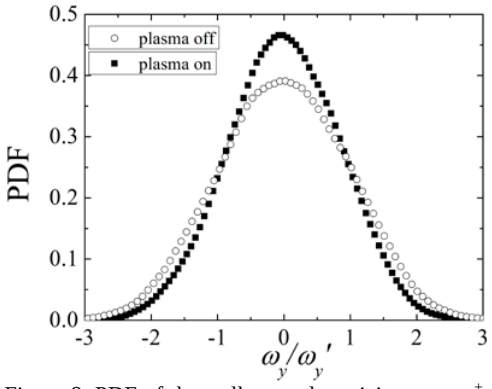

Figure 9. PDF of the wall-normal vorticity ω_y at y^+ = 24 of natural and manipulated turbulent boundary layer.

As shown in Fig. 10, the iso-contours of R_{uu} in the x-y plane (z^+ = 133) are elliptical, with and without control. The inclination angle α of the principal axis of R_{uu} contours is about 9° without control, in good agreement with Liu et al. (2001). The α is the inclination angle of the mean quasi-streamwise vortex (Dritselis & Vlachos, 2008). With control, α decreases to about 4° for the reference points of y^+ = 24 and 40, that is, the angle of the mean quasi-streamwise vortex decreases due to the interaction with plasma-induced vortices. The change in α suggests the suppressed lift-up motion of low-speed streaks and is consistent with the flow visualization results (Fig. 5b), indicating the stabilized low-speed streaks. All those effects point to an interrupted near-wall vortex regeneration cycle. For the reference point of y^+ = 100, however, α is essentially unchanged.

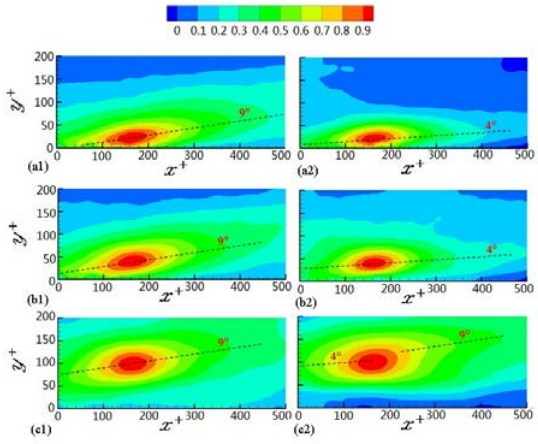

Figure 10. Two-point velocity correlation coefficient R_{uu} in the *x*-*y* plane (z^+ = 133) for plasma off (left column) and on (right column). The reference point is (x^+, y^+) = (167, 24) in (a1, a2), (167, 40) in (b1, b2) and (167, 100) in (c1, c2).

CONCLUSIONS

(1) Preliminary results indicate a maximum drag reduction of about 50% under the configurations A, B, and C, and about 20% under D, which have yet to be verified by further experiments.

(2) There is a pronounced change in the flow structure of the turbulent boundary layer under control, as reflected in the Taylor's microscale, energy dissipation spectrum, the streamwise length and strength of the streaky structures, the orientation of the mean quasi-streamwise vortex decreases from 9° to 4°. The plasma-actuator-induced vortices have made a pronounced effect on the flow structures all the way up to $y^+ \leq 100$. The present results reveal the stabilized low-speed streaks under control, and hence interruption of vortex regeneration cycle, allowing substantial drag reduction.

ACKNOWLEDGMENTS

CW WONG wishes to acknowledge support given to him from Research Grants Council of Shenzhen Government through Grants JCYJ20120613153244545 and JCYJ20130402100505796.

REFERENCES

Bhaganagar, K., Kim, J., and Coleman, G., 2004, "Effect of Roughness on Wall-Bounded Turbulence", *Flow Turbulence and Combustion*, Vol. 72, pp. 463-492.

Choi, K. S., Jukes, T., and Whalley, R., 2011, "Turbulent Boundary-Layer Control with Plasma Actuators", *Philosophical Transactions of the Royal Society of London A: Mathematical, Physical and Engineering Sciences*, Vol. 369, pp. 1443-1458.

Corke, T. C., Enloe, C. L., and Wilkinson, S. P., 2010, "Dielectric Barrier Discharge Plasma Actuators for Flow Control", *Annual Review of Fluid Mechanic*, Vol. 42, pp. 505 – 530.

Dritselis, C. D., and Vlachos, N. S., 2008, "Numerical Study of Educed Coherent Structures in the Near-Wall Region of a Particle-Laden Channel Flow", *Physics of Fluids*, Vol. 20, 055103–055112.

Enloe, C. L., McLaughlin, T. E., VanDyken, R. D., Kachner, K. D., Jumper, E. J., and Corke, T. C., 2004a, "Mechanisms and Responses of a Single Dielectric Barrier Plasma Actuator: Plasma Morphology", *AIAA Journal*, Vol. 42, No. 3, pp. 589–594.

Enloe, C. L., McLaughlin, T. E., VanDyken, R. D., Kachner, K. D., Jumper, E. J., and Corke, T. C., 2004b, "Mechanisms and Responses of a Single Dielectric Barrier Plasma Actuator: Geometric Effects", *AIAA Journal*, Vol. 42, No. 3, pp. 595–605.

Font, G. I., 2006, "Boundary Layer Control with Atmospheric Plasma Discharges", *AIAA Journal*, Vol. 44, No. 7, pp. 1572-1578.

Jukes, T. N., Choi, K. S., Johnson, G. A., and Scott, S. J., 2006, "Characterization of Surface Plasma-Induced Wall Flows Through Velocity and Temperature Measurements", *AIAA Journal*, Vol. 44, No. 4, pp. 764-771.

Krogstad, P. A., and Efros, V., 2010, "Rough Wall Skin Friction Measurements using a High Resolution Surface Balance", *International Journal of Heat and Fluid Flow*, Vol. 31, pp. 429-433.

Liu, Z., Adrian, R. J., and Hanratty, T. J., 2001, "Large-Scale Modes of Turbulent Channel Flow Transport and Structure", *Journal of Fluid Mechanics*, Vol. 559, pp. 83-80.

Metzger, M., 2004, "Length and Time Scale of the Near-Surface Axial Velocity in a High Reynolds Number Turbulent Boundary Layer. *International Journal of Heat and Fluid Flow*, Vol. 27, pp. 534-541.

Mydlarski, L., and Warhaft, Z., 1996, "On the Onset of High-Reynolds-Number Grid-Generated Wind Tunnel Turbulence", *Journal of Fluid Mechanics*, Vol. 320, pp. 331-368.

Moreau, E., 2007, "Airflow Control by Non-Thermal Plasma Actuators", *Journal of Physics D: Applied Physics*, Vol. 40, pp. 605 – 636.

Tardu, S. F., 2001, "Active Control of Near-Wall Turbulence by Local Oscillating Blowing", *Journal of Fluid Mechanics*, Vol. 439, pp. 217-253.